IEEE Robotics and Automation Letters (RA-L) paper, presented at ICRA 2026, Vienna, Austria. Cite as RA-L paper.

Design of a Hydraulic-Driven Adaptive Gripper With a Novel Actuation Mechanism

Yonghwan Jeong, Jungyeong Kim, Sangchul Han, Sungwoon Yoon, Sungho Lee, Sangshin Park, Jin Tak Kim, Jinhyeon Kim, and Jungsan Cho

***Abstract*—This letter presents a novel hydraulic-driven two-finger robotic gripper designed to handle objects of various shapes and sizes. To meet the demands of field robotics and heavy industrial environments, a self-adaptive finger mechanism was integrated with hydraulic actuation. However, this integration leads to increased structural volume, as hydraulics produce linear motion and require additional hydraulics components. Additionally, precise force control becomes challenging, as harsh environments limit the use of other sensing devices for fine control. These issues are addressed by employing an offset slider-crank mechanism, which efficiently converts linear motion into rotational motion. Additionally, a newly designed double-acting bi-piston cylinder allows both fingers to operate using a single cylinder, reducing the number of hydraulic components. To enable pressure-based force control, kinematic and static analyses of the mechanism were conducted. A prototype was developed and experimentally validated for its grasping performance and analysis. It demonstrated high performance in lifting heavy objects, such as an 18 kg tire, and delicately handling fragile items like eggs and paper cups.**

***Index Terms*—Grippers and other end-effectors, mechanism design, hydraulic/pneumatic actuators.**

I. Introduction

As ROBOTS are increasingly used not only in field robotics but also in construction and heavy industries, there is growing demand for grippers capable of complex manipulation tasks. These tasks require not only strong force for heavy objects but also the ability to handle irregularly shaped items.

To address these demands, research on electrically driven grippers has focused on improving their ability to grasp various objects. For example, designs like the ILDA Hand [1] and Robonaut Hand [2] use high degree of freedom(DOF) to perform complex grasping actions [3], [4]. However, as DOF increases, control complexity also rises, making it harder to maintain success rates and safety. Alternatively, research on under-actuated mechanisms reduces complexity and DOF while adapting fingers to object shapes. The self-adaptive finger mechanism (SAFM) [5], [6], [7] is a representative example of an under-actuated structure, in which links and joints are kinematically coupled so that the fingers passively conform to the object. It consists solely of links, gears, and springs, without sensors or soft materials. In SAFM, the actuation link—generally used to transmit actuator force—is driven by motor in this design, causing the remaining links to move in coordination to perform a grasping motion. This design enables simple control and allows for stable grasping of various objects. Sarah Hand [8] and its commercial product, the Robotiq 3-Finger Gripper [9], use multiple 4-bar linkage structures for power grasping and a parallel link structure for pinch grasping [10].

Electric motors used in SAFM simplify implementation by integrating the power source and actuator, but their limited output makes them less suitable for heavy loads. High-reduction gearboxes increase force but also add size and weight, while reducing speed and impact resistance, which limits design flexibility. In contrast, hydraulic systems offer higher power density and strong force, while enabling a more compact gripper by separating the actuator from the power source [11].

This letter identifies the design challenges in implementing a SAFM with hydraulic actuation to achieve both strong grasping and adaptability in field and heavy industrial environments, proposes corresponding solutions, and validates their effectiveness through experiments. To date, no such implementation has been reported, largely due to challenges such as mechanical complexity, increased volume, hydraulic circuit design, and limited force control. We focuses on two issues to improve practical use with manipulators. First, structural volume must be minimized, as it increases wrist torque during heavy lifting and limits performance in tight spaces. Since SAFM requires rotational motion while hydraulics produce linear motion, a compact conversion mechanism is necessary. The inclusion of valves, ports, and

Received 11 February 2025; accepted 3 June 2025. Date of publication 26 June 2025; date of current version 3 July 2025. This article was recommended for publication by Associate Editor C. Piazza and Editor C. Gosselin upon evaluation of the reviewers' comments. This work was supported in part by the Korea Institute of Industrial Technology 'Development of Core Technologies for a Working Partner Robot in the Manufacturing Field under Grant KITECH EO250005 and in part by the R&D Program for Forest Science Technology under Project RS-2024-00403540 through Korea Forest Service (Korea Forestry Promotion Institute. *(Corresponding author: Jungsan Cho.)*

Yonghwan Jeong and Jungsan Cho are with the Hydraulic Robot Laboratory, AI· Robotics R&D Department, Korea Institute of Industrial Technology, Ansan 15588, South Korea, and also with Robotics, University of Science and Technology (UST), Daejon 34113, South Korea (e-mail: jyh960205@gmail.com; chojs@kitech.re.kr).

Jungyeong Kim, Sangchul Han, Sangshin Park, Jin Tak Kim, and Jinhyeon Kim are with the Hydraulic Robot Laboratory, AI· Robotics R&D Department, Korea Institute of Industrial Technology, Ansan 15588, South Korea (e-mail: bomber21@kitech.re.kr; pss@kitech.re.kr; jintagi@kitech.re.kr; qkrb0117@kitech.re.kr).

Sungwoon Yoon and Sungho Lee are with the Hydraulic Robot Laboratory, AI· Robotics R&D Department, Korea Institute of Industrial Technology, Ansan 15588, South Korea, and also with the School of Mechanical Engineering, Sungkyunkwan University, Seoburo 2066, South Korea (e-mail: yoonsw95@skku.edu; dltjdgh56@skku.edu).

This article has supplementary downloadable material available at https://doi.org/10.1109/LRA.2025.3583473, provided by the authors.

Digital Object Identifier 10.1109/LRA.2025.3583473

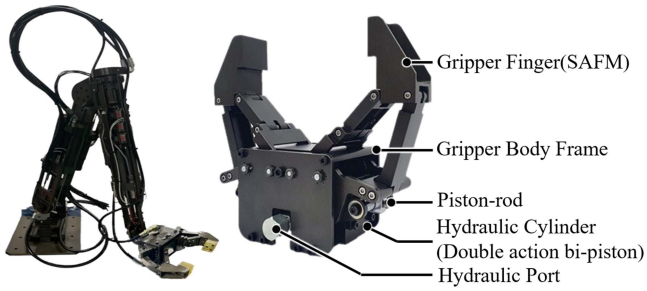

Fig. 1. Proposed hydraulic-driven robotic gripper: the left image shows the gripper integrated with a hydraulic manipulator, and the right image show the names of each mechanism in the gripper.

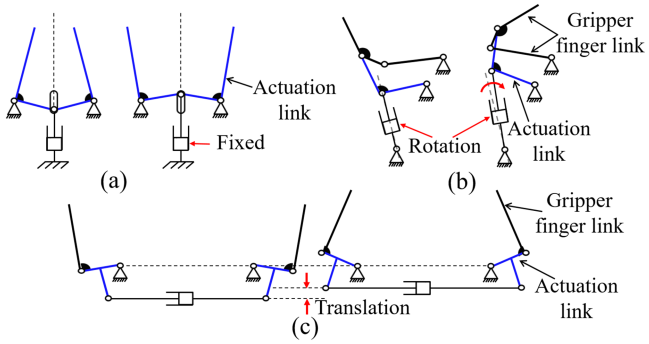

Fig. 2. Examples of mechanisms that convert linear motion to rotational motion in hydraulic-driven grippers. (a) A commonly used structure with a vertically fixed cylinder. (b) The WLRG-II structure, where the cylinder rotates in response to piston movement. (c) A horizontally arranged cylinder to reduce palm length, where the cylinder moves up and down with piston motion.

hoses further increases bulk, making it essential to minimize hydraulic components. Second, precise force control is limited. Unlike electric motors, hydraulic systems are not well-suited for current-based fine force control, and the use of precision sensors is often impractical in harsh environments such as field robotics or construction sites. Therefore, an indirect control method that adjusts grasping force using only pressure—without external sensors—is required.

To reduce structural volume, we propose two solutions. First, an offset-crank mechanism converts the cylinder's linear motion into rotation in a compact space, allowing the cylinder to stay fixed and aligned with the gripper base to shorten overall length. Second, a double-actuated bi-piston cylinder is designed with two pistons and three chambers. Applying pressure to the center chamber closes the fingers; pressure to the outer chambers opens them. Since a single servo valve controls all three chambers, desynchronization motion can occur due to differences in friction or assembly tolerances. To compensate for this, torsion springs are added to passively synchronize the positions of the two pistons. This structure enables two-finger actuation with one cylinder, reducing hydraulic components and minimizing servo valve use. Next, to enable pressure-based grasping force control, we performed analyses of the proposed mechanism. The analysis determined key parameters—cylinder stroke, bore size, and spring constant—and simulated the pressure–force relationship. The prototype successfully grasped various objects, from a 18 kg tire to delicate items like eggs and paper cups.

The paper is organized as follows. Section II explains the design problem statement. Section III explains the design concept. Section IV describes kinematics and statics. In Section V, the gripper shown in Fig. 1 is fabricated to validate the proposed mechanism. Section VI presents experiments to verify performance. Finally, Section VII provides the conclusions and future work.

II. Design Problem Statement

A. Importance of Palm Length and Structural Characteristics of Hydraulic Grippers

Among the factors that determine the gripper volume, the overall length and palm length are particularly influential in task manipulation performance. The palm, situated between the manipulator's wrist joint endpoint and the gripper body's contact point with the object, houses components such as controllers and actuators [12], [13]. As the palm length increases—that is, as the vertical distance from the manipulator's connection point to the gripper body's contact point becomes longer—the wrist joint requires larger movements to control the orientation and position of the end effector [14]. This hinders operation in confined spaces, increases wrist torque requirements, and leads to design challenges. In designing gripper, our primary objective is to reduce the overall volume by minimizing the palm length. To achieve this, we analyze existing hydraulic-driven grippers structure and propose a mechanism to address these challenges.

Fig. 2(a) [15] shows a commonly used design. Its simplicity and minimal force loss make it suitable for heavy loads. However, the limited rotational range, restricts its applicability. Fig. 2(b) shows the WLRG-II [16] mechanism, where the actuation link rotates according to the piston, and the gripper finger link rotates at a larger ratio, compensating for the limited rotational range. The additional DOF of the finger link allows for flexible movement, adapting to the object's shape. However, these structures lead to an increased palm length due to the vertically arranged actuator. To address this issue, the structure in Fig. 2(c) [17] arranges the cylinder horizontally. The cylinder moves upward and downward in line with the piston motion, while the actuation link rotates around a fixed joint. By arranging the cylinder horizontally, this structure reduces palm length compared to previous designs. However, the cylinder is not fixed and moves, requiring additional space for movement. Moreover, the stiffness of the high-pressure hydraulic hoses can hinder the cylinder motion. Based on this analysis, we developed a transformation mechanism that adopts a horizontally fixed cylinder arrangement to minimize the palm's length.

B. Piston Desynchronization in a Proposed Cylinder

Generally, two-finger grippers are designed to move both fingers simultaneously to improve object grasping success rates. This is typically achieved through mechanical methods such as gears or linkages or by using position sensors to control each joint. If the fingers do not move simultaneously, the first finger to contact the object may displace it, causing issues [18]. The hydraulic circuit of the proposed cylinder is the same as

IEEE Robotics and Automation Letters (RA-L) paper, presented at ICRA 2026, Vienna, Austria. Cite as RA-L paper.

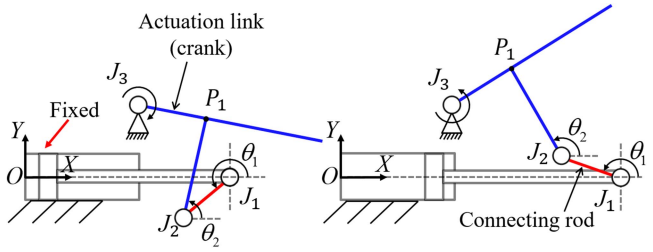

Fig. 3. Actuation mechanism with offset slider-crank. (a) The gripper opening mechanism in response to piston movement in the x^- direction. (b) The gripper closing mechanism in response to piston movement in the x^+ direction

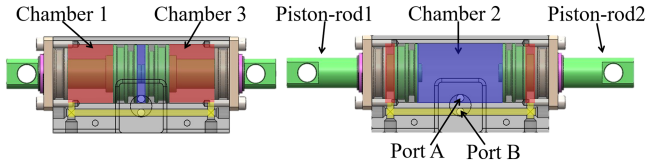

Fig. 4. Double actuated bi-piston cylinder. (a) Operation of the piston rods moving toward the center. (b) Operation of the piston rods moving apart.

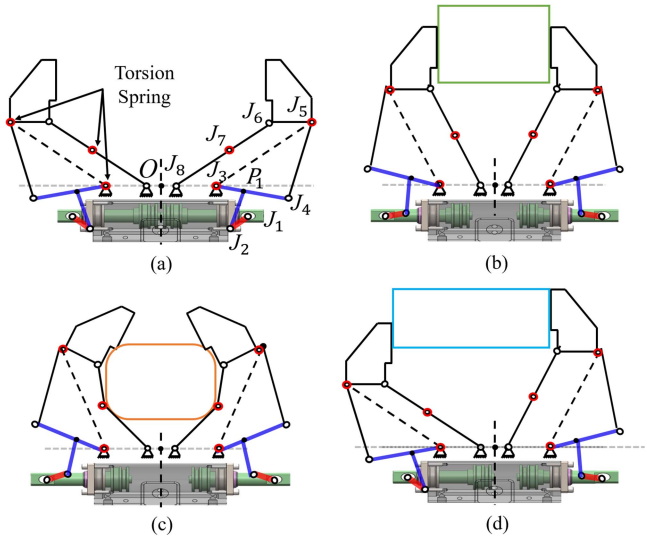

Fig. 5. Gripper mechanism with the proposed hydraulic cylinder. (a) Initial state. (b) Pinch grasping. (c) Power grasping. (d) Off-Centered Object Grasping.

that used to connect two double-acting cylinders to a single valve. Ideally, identical machining tolerances and simultaneous valve input would allow the pistons to advance together. In practice, differences in friction and machining errors cause the piston with lower friction to move first. Therefore, a method to ensure synchronization between the two pistons is required. We aim to passively correct the piston position difference without additional sensors or actuators.

III. Design

A. Concept of Gripper Link Mechanism

The motion conversion structure is based on the horizontally arranged cylinder (Fig. 2(c)), which typically allows cylinder movement. To resolve this, the proposed design fixes the cylinder to restrict its vertical movement and incorporates an additional link to form a new structure, as shown in Fig. 3. This structure can be considered a typical offset slider-crank mechanism. In this mechanism, the actuation link(blue) acts as the crank, the piston of the cylinder as the slide, and the link(red) as the connecting rod. The connecting rod's motion range is determined by the kinematic interaction between the actuation link and the piston of the cylinder. The operating angle, θ_1, ranges from 90° to 270°, ensuring that issues such as free motion or jamming do not occur, provided $\theta_1 \neq \theta_2$.

The mechanism operates as the crank rotates about point J_3 in response to piston movement. When the piston moves in the x^+ direction, J_1 is pulled, and the actuation link rotates clockwise around J_3, closing the gripper, as shown in Fig. 3(a). Conversely, when the piston moves in the x^- direction, J_1 is pushed, causing the actuation link to rotate counterclockwise and opening the gripper, as shown in Fig. 3(b). This mechanism converts linear motion into rotational motion, and the fixed cylinder design minimizes palm length by eliminating the need for high-pressure hydraulic line or port movement.

B. Double Actuated Bi-Piston Cylinder

We propose a new hydraulic actuator design that drives both fingers with a single actuator. The double-acting bi-piston cylinder is shown in Fig. 4. The proposed actuator consists of two piston-rod and three chambers inside a single cylinder body. This design is based on the concept of both fingers of a two-finger gripper moving simultaneously, either opening or closing, with the pistons of the two cylinders moving in opposite directions. The structure integrates two cylinders placed side by side into one, allowing the pistons to operate in opposing directions. Fluid entering Port B flows along the yellow hydraulic line into Chambers 1 and 3 (marked in red), pulling the pistons toward the center, as shown in Fig. 4(a). The working fluid entering Port A moves into Chamber 2 (marked in blue), pushing the pistons apart, as shown in Fig. 4(b). This integrated structure reduces the number of components required for cylinder manufacturing, including hydraulic ports and seals, resulting in a smaller overall volume. Additionally, the number of valves needed for control is reduced, simplifying the control system. In addition, the cylinder allows each piston to respond independently to resistance. This characteristic allows one finger to stop first while the other continues to move, enabling the grasping motion to be completed without additional control.

Fig. 5 shows the gripper mechanism, which integrates the motion conversion structure, the proposed cylinder, and the SAFM. The SAFM consists of links and torsion springs, enabling both pinch and power grasping. Solid lines in Fig. 5 represent SAFM links, while dashed lines indicate imaginary lines for explanatory purposes. Black circles (J_1, J_2, J_4, J_6, J_8) represent joints, and red-black circles (J_3, J_5, J_7) denote joints with torsion springs. The cylinder's rod end connects to J1. The gripper's basic operating principle is to maintain the virtual parallelogram formed by J_3, J_5, J_6, and J_8 using the torsion spring forces at

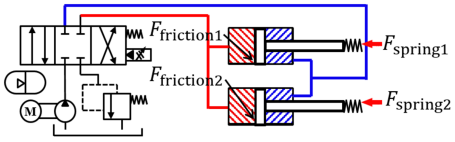

Fig. 6. Addition of springs to each cylinder rod to ensure synchronization of piston movement.

joints J_5 and J_7. When no external force is applied to the J_6-J_7 and J_7-J_8 links, the hydraulic cylinder's piston motion rotates the J_3-J_4 link, maintaining the SAFM's parallelogram shape. In this state, as shown in Fig. 5(b), the gripper securely grasp objects using pinch grasping. Conversely, when an external force is applied to the J_6-J_7 and J_7-J_8 links, the link angles adjust to the object's shape, as shown in Fig. 5(c). When releasing the object, the torsion springs at J_5 and J_7 restore the SAFM to its original parallelogram configuration. Fig. 5(d) shows a case where one finger contacts the object first, remains stationary, and the opposite finger continues rotating to complete the grasp. This behavior demonstrates effective grasping even when the object is off-center or has an irregular shape.

C. Synchronization Between Two Fingers

To address this, adding orifices or on/off valves to the hydraulic circuit could be considered. Instead, the proposed approach addresses the issue using a simpler structure and control mechanism. As shown in Fig. 6, springs are added in front of each cylinder rod, providing reactive force based on piston position in addition to cylinder friction. These springs adjust piston speeds, ensuring synchronization between the two pistons. The relationship between the spring constant and the piston's displacement is described by (1).

$$k = \frac{F_{\text{friction1}} - F_{\text{friction2}}}{\Delta X} \tag{1}$$

Here, ΔX represents the distance between the two cylinders, and friction1 and friction2 denote the friction forces of Cylinder1 and Cylinder2, respectively. It is assumed that spring1 and spring2 have the same spring constant k. The value of k is determined by the measured friction forces of the cylinders and the desired distance ΔX between them. After installing the springs with the calculated k, the operation is as follows: Initially, a force F, generated by pressure P, is applied. If the friction force of Cylinder2 is smaller, Cylinder2 begins to move first. During this process, the spring's deformation generates a force, redirecting the fluid to Cylinder1's chamber, which has lower pressure. Once the pressure exceeds friction1, Cylinder1 begins to move, maintaining a consistent distance between the Cylinder2.

IV. Analysis

A. Kinematics of Grasping Motion

This section defines the kinematic relationship between the rod end position and the gripper links based on the size of the object being grasped. Kinematic equations are derived for two

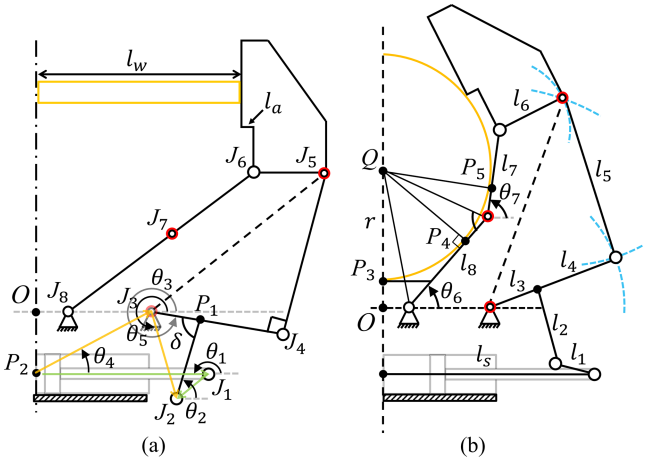

Fig. 7. Geometric parameters of the gripper mechanism. (a) Pinch grasping. (b) Power grasping.

TABLE I
Gripper Design Parameters

Parameter	Value
θ_1	$\sin^{-1}\left(\frac{l_9\sin(\theta_4)+l_{10}\sin(\theta_5)}{l_1}\right)$
θ_2	$\theta_3+\delta-2\pi$
θ_3	$\sin^{-1}\left(\frac{l_2\sin(\delta)}{l_{10}}\right)+\theta_5$

cases: pinch grasping of a rod-shaped object and power grasping of a cylindrical object. Fig. 7 shows the geometric parameters of the proposed mechanism. l_i represents the link lengths between joints, l_a is a constant. θ_i is the angle measured counterclockwise from the x-axis. J_{ix} and J_{iy} are the coordinates of the point J from the origin O, and δ represents $\angle J_3P_1J_2$. P_i denotes a contact or joint point, and θ_4 is fixed due to the stationary joint J_3. l_s is the rod-end position, l_w is the fingertip position corresponding to the rod-shaped object length, and r is the radius of the cylindrical object.

To analyze pinch grasping kinematics in Fig. 7(a), a virtual four-bar linkage is formed by P_2, J_3, J_2, and J_1, connected by yellow and green arrows. The geometric relationships of each link can be expressed using a vector loop diagram, which is formulated as follows:

$$\overrightarrow{P2J3} + \overrightarrow{J3J2} = \overrightarrow{P2J1} + \overrightarrow{J1J2} \tag{2}$$

By decomposing the vector loop (2) into geometric components along the x- and y-axes, the angle θ_5 of the virtual vector $\overrightarrow{J_3J_2}$ can be calculated. Subsequently, θ_1, θ_3, and θ_2 are obtained sequentially. The results are summarized in Table I.

Finally, based on the calculated values of θ_i and the link lengths, l_w was derived as shown in (3). This equation represents l_w as a function of l_s based on the geometric relationships between links and joints.

$$\begin{aligned} l_w = {} & l_1\cos(\theta_1) + l_2\cos(\theta_2) + l_4\cos(\theta_3) \\ & + l_5\cos\left(\theta_3+\frac{\pi}{2}\right) - l_6 - l_a + l_s \end{aligned} \tag{3}$$

IEEE Robotics and Automation Letters (RA-L) paper, presented at ICRA 2026, Vienna, Austria. Cite as RA-L paper.

Next, as shown in Fig. 7(b), the relationship between the cylindrical object's radius r and the rod end position is analyzed for power grasping. Regarding the bent link J_7J_8 that contacts the cylindrical object, the position of point J_7 is determined by first calculating the interior angle of triangle QJ_8J_7 using the law of cosines, from which the angle θ_6 is obtained. The following equations summarize this process:

$$\theta_6 = \pi - \tan^{-1}\left(\frac{r + \overline{OP_3}}{J_s}\right) - \angle QJ_8J_7$$
$$J_7 = [J_s,\ 0] + [l_8\cos(\theta_6),\ l_8\sin(\theta_6)] \tag{4}$$

Subsequently, using the law of cosines and the previously calculated angle θ_6, the angle θ_7 is calculated. Based on this value, the position of point J_6 is determined. J_5 is geometrically determined as the intersection point of two circles centered at J_6 and J_3, with radii l_6 and $l_7 + l_8$, respectively. J_4 is calculated in the same way. Typically, two intersection points exist between the circles. Among them, the point located farther in the positive x-direction is selected based on a predefined condition. As shown in Fig. 7(b), the blue dashed line visually indicates only the selected intersection point. Based on the calculated position of J_4, J_2 is given by:

$$J_2 = J_3 + [l_3\cos(\theta_3),\ l_3\sin(\theta_3)] + [l_2\cos(\phi),\ l_2\sin(\phi)] \tag{5}$$

where ϕ is defined as $\phi = \pi + \delta + \theta_3$. Finally, given that the distance between J_1 and J_2 is fixed and the y-position of the rod end is constrained, the x-position of the rod end l_s is calculated using the following equation:

$$l_s = J_{1x} = J_{2x} + \sqrt{J_1J_2^2 - (J_{2y} - P_{2y})^2} \tag{6}$$

B. Statics of Pinch Grasping Motion

In this section, static analysis is conducted to calculate the pinch grasping force at the fingertip of the proposed gripper based on the pump's supply pressure. The free-body diagram(FBD) of the proposed gripper is shown in Fig. 8. The thrust of the cylinder is defined by f_a, and the pushing force exerted by the fingertip is represented as f_e. The interaction forces at the joints of each link are represented as $f_{\alpha\beta}$.

The equations of motion for the link including joint J1, resulting from the cylinder's thrust f_a, satisfy the following:

$$\sum F_x = f_a + f_{12}\cos(\theta_1) = 0 \tag{7}$$

For the J_1J_2 link, force equilibrium is considered in both x- and y-directions. For the $J_2J_3J_4$ link, using $f_{23x} = -f_{32x}$ and $f_{23y} = -f_{32y}$, T_{J3} and f_{34} are derived as follows:

$$\sum T_{J3} = f_{32x}J_{2y} - f_{32y}J_{2x} - f_{34}(l_3 + l_4) - K_s\Delta\theta_3 = 0 \tag{8}$$

where $K_s\Delta\theta_3$ represents the force exerted by the torsion spring.

For the J_5J_6 link,using $f_{34} = -f_{43}$, $f_{43} = -f_{45}$ and $f_{45} = -f_{54}$, T_{J6} and f_e are derived as follows:

$$\sum T_{J6} = -f_el_e + f_{54y}l_6 = 0 \tag{9}$$

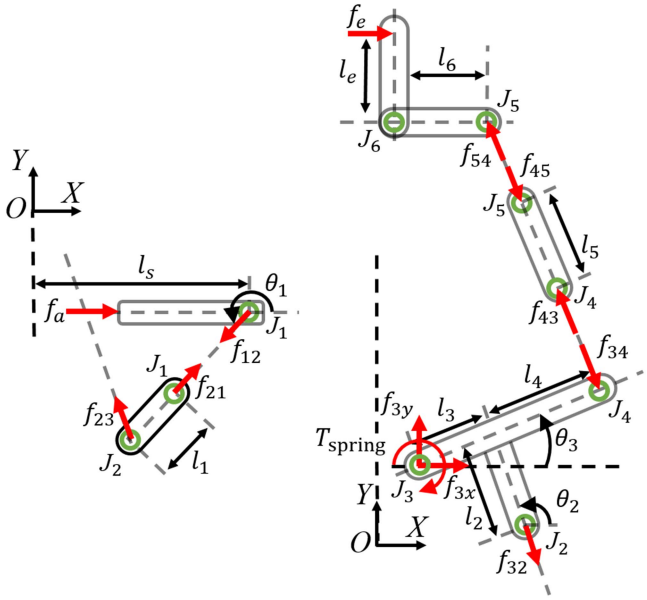

Fig. 8. FBD of the proposed gripper.

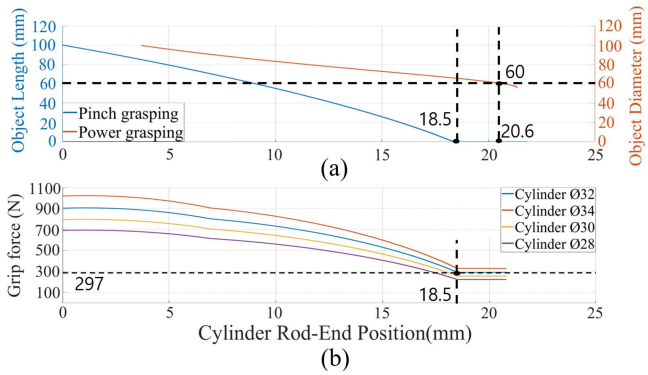

Fig. 9. Calculated value. (a) Relationship between Cylinder stroke and graspable object size. (b) Grip force according to cylinder rod-end position and size.

$$f_e = \frac{\cos(\theta_3)l_6}{(l_3 + l_4)l_e}\left[-K_s\Delta\theta_3 + (J_{2y} - \tan(\theta_1)J_{2x})\, f_a\right] \tag{10}$$

V. Mechanical Implementation

A. Design Parameter Determination

This section determines the cylinder stroke, bore size, and spring constant to meet the design objectives of the proposed gripper. The gripper is designed to provide a pinch grasping force over 294 N(30 kgf) at 30 bar, grasp objects up to 100 mm, and perform power grasping for cylindrical objects with a minimum diameter of 60 mm.

First, using the kinematic analysis results from (3) and (6), the relationship between cylinder stroke and object length was derived for both pinch and power grasping. Fig. 9(a) shows the required stroke as a function of object length. The analysis indicates that a stroke of approximately 18.5 mm is needed

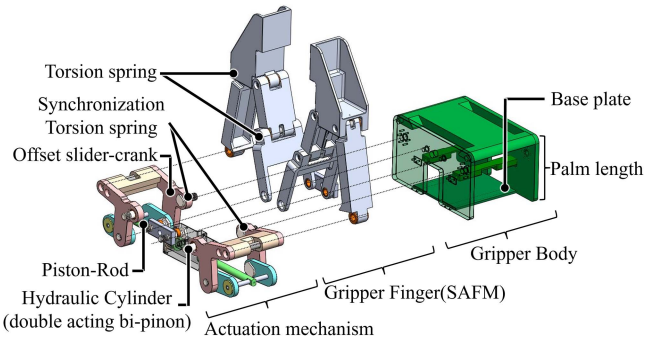

Fig. 10. Exploded view of gripper design.

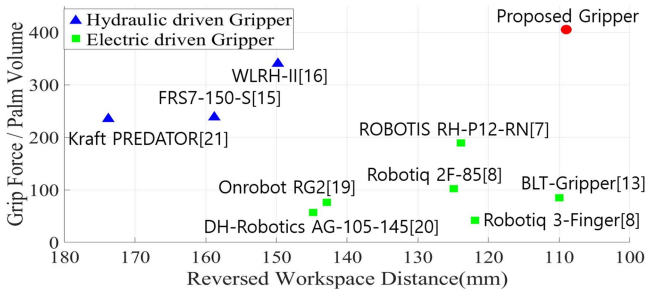

Fig. 11. Performance comparison of grippers. Hydraulic grippers [12], [15], [19] are shown as blue triangles, electric grippers [7], [9], [13], [20], [21] as green squares, and the proposed gripper as a red circle.

to perform pinch grasping on a 100 mm rod-shaped object, and about 20.6 mm for power grasping a 60 mm cylindrical object. Based on this, the cylinder stroke was set to 21 mm. Next, Fig. 9(b) shows the variation of pinch grasping force with rod-end position for different cylinder bore sizes. According to simulation results using the static analysis (10), approximately 294 N of grasping force is generated at a rod end position of 18.5 mm—corresponding to the completion of pinch grasping—when using a cylinder with a Ø 32 bore. Thus, the bore size was set to Ø 32 to meet the design criteria.

Finally, to compensate for positional differences between the two pistons, a push-pull gauge measured a friction difference. Based on this measurement, a torsion spring made of 1.6 t spring steel was selected to maintain the distance between the pistons within 2 mm, satisfying a spring constant of 14Nmm/deg calculated using equations (1) and (8). The energy required to actuate each torsion spring is approximately 0.2696 J, based on a rotation angle of $\Delta\theta = 47^{\circ}$, and the total energy stored in both springs is about 0.5392 J. Meanwhile, under a supply pressure of 30 bar, the cylinder exerts approximately 50.6520 J of mechanical energy over a stroke length of 21 mm. Thus, the spring energy accounts for only about 1% of the total input. Nevertheless, the torsion springs effectively compensate for the positional offset between the pistons, ensuring reliable synchronization.

B. Fabrication and Specification Comparison

This section describes the prototype specifications of the proposed gripper and evaluates its design efficiency through a comparison with existing commercial grippers. Fig. 10 shows the 3D exploded view of the gripper, which consists of a double-acting bi-piston cylinder with an offset slider-crank in the actuation mechanism, an SAFM-based finger part, and the main body. The gripper's dimensions are 180 mm × 206 mm × 93 mm (L× W× D), and it weighs 1.9 kg. The body frame and links are made of aluminum, while the pistons and shafts are made of steel to ensure high strength and durability. The torsion springs for synchronization are located at joint J3, which is positioned between the actuation mechanism and the gripper body. The cylinder has a piston diameter of 32 mm and a rod diameter of 16 mm. To prevent potential leakage during operation and ensure smooth linear motion of the cylinder, Glide Ring (Trelleborg) and Wear Ring (Trelleborg) were used. Bushings were applied to each joint to ensure stable operation under high loads and to reduce friction and wear between components, thereby maintaining long-term durability. Compared to needle bearings, the smaller outer diameter of the bushings allows for a more compact design. Torsion springs with a spring constant of 8 N·mm/deg, made of 1.2 t piano wire, were applied to each finger. The spring constant was selected to provide sufficient restoring force for stable power grasping of heavy objects.

Fig. 11 compares the proposed gripper with various electric and hydraulic grippers. Due to differing sizes and structures, relative ratios were used to assess structural efficiency. The horizontal axis represents the reversed workspace [14] distance, which refers to the estimated space required for manipulation when the gripper is assumed to be mounted on a specific wrist mechanism. In this study, the metric is calculated based on a human wrist model, with the palm length normalized accordingly. A larger reversed workspace distance implies that more space is required when operating the gripper in conjunction with a manipulator, while smaller values suggest better performance in confined environments. Hydraulic grippers typically show higher values due to cylinder linear motion and components like ports and valves. In contrast, the proposed gripper shows the lowest ratio, even compared to electric grippers that adopt the same SAFM mechanism. The vertical axis reflects force relative to palm volume, serving as an indicator of actuator power density. As hydraulic systems offer higher power density than electric ones, they tend to show greater values. By achieving both a compact structure and hydraulic output, the design proves its effectiveness.

VI. Experimental Validation

To evaluate the performance of the proposed gripper, four experiments were conducted. First, the synchronization performance of the hydraulic cylinder was tested by measuring the pistons position changes. Second, the static analysis was validated through open-loop grasping tests, and based on the analysis results, pressure feedback control was applied to experimentally demonstrate force control of pinch grasping without using touch sensors. Third, an experiment was conducted to observe the characteristic behavior of the proposed cylinder during grasping. Lastly, grasping tests with various objects confirmed the gripper's stability and applicability. The hydraulic system used

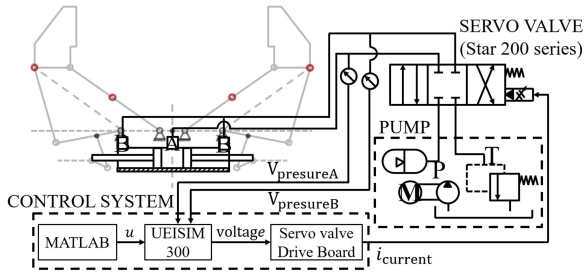

Fig. 12. Control and experimental configuration of a hydraulic gripper.

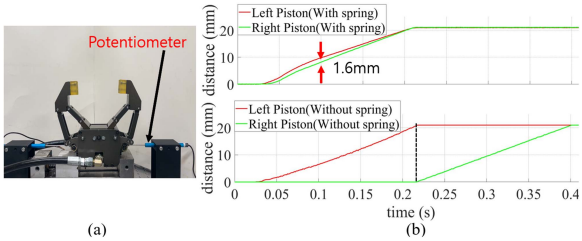

Fig. 13. Verification of the synchronization performance. (a) Experimental setup. (b) Piston position measurement results.

in the experiments is shown in Fig. 12. The hydraulic supply source provides a flow rate of up to 30 liters per minute, with pressure controlled between 0 and 210 bar. The control system was implemented using Matlab and UEISIM(United Electronic Industries). Pressure was measured from sensor voltage via ADC, and DAC signals drove a custom servo valve circuit. This circuit controlled the flow rate by operating an electric hydraulic servo valve, 200 series(Star Hydraulics). Pressure sensor(LUMAX) signals were collected through an ADC.

A. Evaluation of the Synchronization Performance

To evaluate synchronization, positional changes of both pistons were measured during cylinder operation, as shown in Fig. 13(a). The SLS095(CURTISS-WRIGHT) potentiometer, aligned with both pistons, was used to measure the position of the pistons. Fig. 13(b) shows the measurement results. In the upper graph of Fig. 13(b), where the torsion spring was applied, the two pistons moved almost simultaneously, and the maximum positional difference was approximately 1.6 mm, satisfying the design target of less than 2 mm. In contrast, in the lower graph of Fig. 13(b) without the spring, the piston with less friction started moving first, followed by the other piston, showing a clear asynchronous motion and a large positional deviation. These results demonstrate that the torsion spring improved the synchronization performance by compensating for the positional difference. The inconsistent positional difference between the two pistons were attributed to the nonlinear characteristics, with the positional difference increased or decreased in certain regions.

B. Evaluation of Pinch Grasping Force Analysis

The experiment consisted of two parts. The first part measured the pinch grasping force according to variations in object length

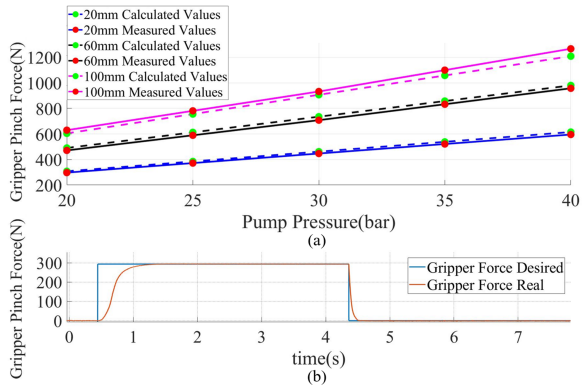

Fig. 14. Pinch grasping force measurement. (a) Comparison of experimental and calculated forces. (b) Pinch grasping force via pressure control.

and pump pressure to evaluate the accuracy of the modeling by comparing it with the calculated values. The second part verified the control of the pinch grasping force through pressure control. The CWFS-200 load cell (BONGSHIN), capable of measuring up to 1960 N, was used to measure the grasping force, and its output signals were processed through the UEISIM system. An ABS-made jig was employed to adjust the length of the objects during the experiment. The experiment was conducted using three jigs. Pump pressure was increased from 20 to 40 bar in 5-bar increments, with five tests conducted at each stage, and the average values measured. Fig. 14(a) presents the results: pink, black, and blue lines represent grasping forces for 100 mm, 60 mm, and 20 mm objects, respectively. Red dots and solid lines indicate measured values, while green dots and dashed lines show calculated values. The average error across the five repeated measurements was within $\pm 1\%$. The error between the calculated and measured values, ranging from 3% to 5%, is attributed to factors such as the frictional force of the bushings and the initial angular difference of the torsion spring.

Fig. 14(b) shows the force control performance of the proposed mechanism based on its analytical model. The target grasping force was set to 294 N, and a 60 mm jig with a load cell was used for validation. The cylinder pressure was controlled via a servo valve using flow regulation. The blue line represents the desired force, and the orange line shows the measured force. These results confirm that the proposed hydraulic gripper enables stable and force-controllable grasping across various object types.

C. Grasping Motion With Off-Centered Object Placement

An experiment was conducted to observe how the proposed cylinder structure operates during off-center object placement. Fig. 15 shows a sequence of images capturing the grasping motion. In the experiment, a wooden block was placed off-center relative to the gripper, so that one finger would make contact with the object first. This setup simulates a situation in which an object is either unaligned with the gripper or has an irregular shape. Once the gripper is actuated, the first contacting finger remains stationary while the other finger continues to rotate to

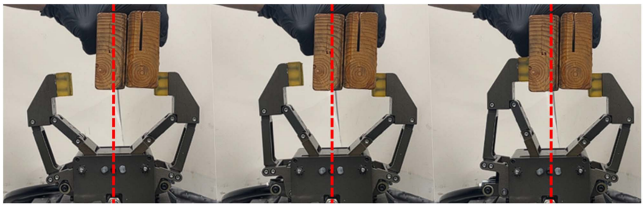

Fig. 15. Grasping an off-centered object using the proposed gripper.

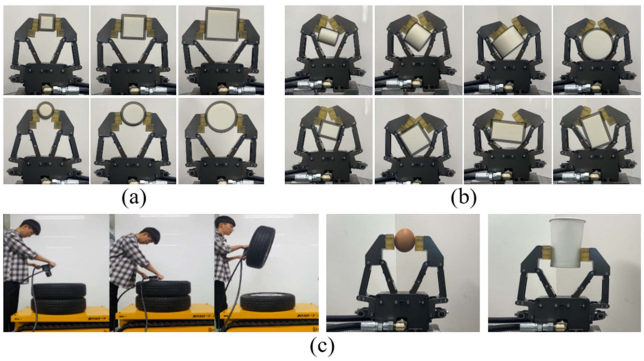

Fig. 16. Grasping experiment results. (a) Pinch grasping of 20 mm, 60 mm, and 100 mm objects (left to right). (b) Power grasping of 20 mm, 60 mm, and 100 mm objects, including a second 100 mm object at a different angle. (c) Grasping tests with various real-world objects.

complete the grasp. This result demonstrates that the proposed mechanism can effectively adapt to unaligned objects without requiring additional sensors or complex control, confirming its flexibility under various grasping conditions.

D. Evaluation of Grasping Performance With Various Objects

Lastly, grasping tests with various objects were conducted to verify performance. The test set included square and cylindrical jigs (20 mm, 60 mm, 100 mm), a 18 kg tire, and fragile items like an egg and paper cup. Tests were divided into pinch grasping for delicate handling and power grasping for heavy loads. Fig. 16(a) shows stable pinch grasping of various shapes and sizes, including a 100 mm target. Fig. 16(b) presents power grasping results, where the finger adapted to a 60 mm cylinder, consistent with the analysis. Fig. 16(c) shows tests with real objects: the gripper lifted an 18 kg tire via SAFM-based power grasping, and delicately performed pinch grasping of an egg and a paper cup using pressure control without damage. The demo video includes tests with bricks and vices, including the lifting of a 20 kg brick using a hydraulic manipulator.

VII. Conclusion

This letter presented a novel hydraulic-driven robotic gripper incorporating a SAFM and converting structure and a double-acting bi-piston cylinder for grasping objects of varying shapes and sizes. The proposed design introduces an offset slider-crank mechanism and a double-acting bi-piston structure. These features minimized palm volume and length while reducing the number of hydraulic components. Synchronization between the two gripper fingers was achieved using torsion springs, ensuring stable operation without additional control components. The fabricated prototype validated the kinematic and static analysis results through experiments. The gripper successfully lifted an 18 kg tire, highlighting high force and stability, and handled fragile objects like eggs and paper cups without damage, showcasing its versatility in both strong and delicate tasks. Future work will focus on force adaptability control only using pressure sensor, investigating the effects of pump pressure and flow for synchronizing cylinder pistons.

References

[1] U. Kim et al., "Integrated linkage-driven dexterous anthropomorphic robotic hand," *Nature Commun.*, vol. 12, no. 1, pp. 1–13, 2021.
[2] C. Lovchik and M. A. Diftler, "The robonaut hand: A dexterous robot hand for space," in *Proc. IEEE Int. Conf. Robot. Automat.*, 1999, pp. 907–912.
[3] S. Jacobsen, E. Iversen, D. Knutti, R. Johnson, and K. Biggers, "Design of the utah/m.i.t. dextrous hand," in *Proc. 1986 IEEE Int. Conf. Robot. Automat.*, 1986, pp. 1520–1532.
[4] D. Chu et al., "Human palm performance evaluation and the palm design of humanoid robotic hands," *IEEE Robot. Automat. Lett.*, vol. 9, no. 3, pp. 2463–2470, Mar. 2024.
[5] D. Yoon, G. Lee, S. Lee, and Y. Choi, "Underactuated finger mechanism for natural motion and self-adaptive grasping towards bionic partial hand," in *Proc. 6th IEEE Int. Conf. Biomed. Robot. Biomechatronics*, 2016, pp. 548–553.
[6] C. Luo and W. Zhang, "VGS hand: A novel hybrid grasping modes robot hand with variable geometrical structure," *Appl. Sci.*, vol. 9, no. 8, 2019, Art. no. 1566.
[7] ROBOTIS, "Robotis RH-P12-RN," Accessed: 2025. [Online]. Available: https://www.robotis.com/shop/
[8] T. Laliberte, L. Birglen, and C. Gosselin, "Underactuation in robotic grasping hands," *Mach. Intell. Robotic Control*, vol. 4, no. 3, pp. 1–11, 2002.
[9] Robotiq, "3-Finger adaptive robot gripper," Accessed: 2025. [Online]. Available: https://robotiq.com/products/3-finger-adaptive-robot-gripper
[10] T. Feix, J. Romero, H.-B. Schmiedmayer, A. M. Dollar, and D. Kragic, "The GRASP taxonomy of human grasp types," *IEEE Trans. Hum.-Mach. Syst.*, vol. 46, no. 1, pp. 66–77, Feb. 2016.
[11] J. Park, J. Lee, H.-T. Seo, and S. Jeong, "Variable transmission mechanisms for robotic applications: A review," *IEEE Robot. Automat. Mag.*, vol. 32, no. 2, pp. 167–188, Jun. 2025.
[12] J. Qi, X. Li, Z. Tao, H. Feng, and Y. Fu, "Design and control of a hydraulic driven robotic gripper," in *Proc. IEEE Int. Conf. Robot. Biomimetics*, 2021, pp. 398–404.
[13] Y.-J. Kim, H. Song, and C.-Y. Maeng, "BLT gripper: An adaptive gripper with active transition capability between precise pinch and compliant grasp," *IEEE Robot. Automat. Lett.*, vol. 5, no. 4, pp. 5518–5525, Oct. 2020.
[14] F. Negrello, S. Mghames, G. Grioli, M. Garabini, and M. G. Catalano, "A compact soft articulated parallel wrist for grasping in narrow spaces," *IEEE Robot. Automat. Lett.*, vol. 4, no. 4, pp. 3161–3168, Oct. 2019.
[15] FOUK, "Fouk FRS7," Accessed: 2025. [Online]. Available: https://foukgripper.com/Grasping-system-8/
[16] Z. Tao, X. Li, H. Feng, and Y. Fu, "Design and control of a novel hydraulic-driven humanoid hand," *Int. J. Humanoid Robot.*, vol. 21, no. 03, 2024, Art. no. 2350015.
[17] J. T. Kim et al., "Development of disaster-responding special-purpose machinery: Results of experiments," *J. Field Robot.*, vol. 39, no. 6, pp. 783–804, 2022.
[18] A. Kobayashi, J. Kinugawa, S. Arai, and K. Kosuge, "Design and development of compactly folding parallel open-close gripper with wide stroke," in *Proc. 2019 IEEE/RSJ Int. Conf. Intell. Robots Syst.*, 2019, pp. 2408–2414.
[19] PREDATOR Kraft, "Kraft predator," Accessed: 2025. [Online]. Available: http://krafttelerobotics.com/products/predator.htm
[20] Onrobot, "Onrobot RG2," Accessed: 2025. [Online]. Available: https://onrobot.com/en/products/rg2-gripper
[21] DHrobot, "Dhrobot AR," Accessed: 2025. [Online]. Available: https://en.dh-robotics.com/product/ag